Simultaneous Activation of Mu and Delta Opioid Receptors Reduces Allodynia and Astrocytic Connexin 43 in an Animal Model of Neuropathic Pain

Nunzio Vicario[1] · Lorella Pasquinucci[2] · Federica M. Spitale[1] · Santina Chiechio[3,4] · Rita Turnaturi[2] · Filippo Caraci[3,4] · Daniele Tibullo[5] · Roberto Avola[5] · Rosario Gulino[1] · Rosalba Parenti[1] · Carmela Parenti[3]

Abstract

Neuropathic pain is a chronic condition triggered by lesions to the somatosensory nervous system in which pain stimuli occur spontaneously or as pathologically amplified responses. In this scenario, the exchange of signaling molecules throughout cell-to-cell and cell-to-extracellular environment communications plays a key role in the transition from acute to chronic pain. As such, connexin 43 (Cx43), the core glial gap junction and hemichannel-forming protein, is considered a triggering factor for disease chronicization in the central nervous system (CNS). Drugs targeting μ opioid receptors (MOR) are currently used for moderate to severe pain conditions, but their use in chronic pain is limited by the tolerability profile. δ opioid receptors (DOR) have become attractive targets for the treatment of persistent pain and have been associated with the inhibition of pain-sustaining factors. Moreover, it has been shown that simultaneous targeting of MOR and DOR leads to an improved pharmacological fingerprint. Herein, we aimed to study the effects of the benzomorphan ligand LP2, a multitarget MOR/DOR agonist, in an experimental model of neuropathic pain induced by the unilateral sciatic nerve chronic constriction injury (CCI) on male Sprague-Dawley rats. Results showed that LP2 significantly ameliorated mechanical allodynia from the early phase of treatment up to 21 days post-ligatures. We additionally showed that LP2 prevented CCI-induced Cx43 alterations and pro-apoptotic signaling in the CNS. These findings increase the knowledge of neuropathic pain development and the role of spinal astrocytic Cx43, suggesting new approaches for the treatment of neuropathic pain.

Keywords Chronic constriction injury · LP2 · Astrocytes · Gap junction · Spinal cord

Nunzio Vicario and Lorella Pasquinucci contributed equally to this work.

Electronic supplementary material The online version of this article (https://doi.org/10.1007/s12035-019-1607-1) contains supplementary material, which is available to authorized users.

✉ Rosalba Parenti
parenti@unict.it

1 Department of Biomedical and Biotechnological Sciences, Section of Physiology, University of Catania, 95123 Catania, Italy

2 Department of Drug Sciences, Section of Medicinal Chemistry, University of Catania, 95125 Catania, Italy

3 Department of Drug Sciences, Section of Pharmacology and Toxicology, University of Catania, 95125 Catania, Italy

4 Oasi Research Institute—IRCCS, 94018 Troina, Italy

5 Department of Biomedical and Biotechnological Sciences, Section of Biochemistry, University of Catania, 95123 Catania, Italy

Introduction

Neuropathic pain is a pathological chronic condition, resulting from injuries to the peripheral or central nervous system (CNS), characterized by altered transmission and modulation of nociception [1]. In chronic neuropathic disorders, decreased inhibitory influence at spinal level and central sensitization are associated with several molecular changes resulting in pro-nociceptive facilitation [2, 3]. Unfortunately, the molecular mechanisms involved in the transition from acute to chronic pain and potential targets of neuropathic pain are not fully elucidated. A number of studies have pointed out the crucial role of spinal glia in sustaining inflammation and neuropathy development [4, 5] and maintenance through the release of astroglial mediators, increasing the activity of nociceptive neurons [6, 7]. Astrocytes in the adult CNS participate to the networking mechanisms also by gap junctions and hemichannels, to exchange cytosolic content between adjacent cells and

to the extracellular space, respectively. Connexin 43 (Cx43), the core glial gap junction and hemichannel-forming protein, is the main astrocytic connexin of the CNS [8, 9]. In the spinal cord, Cx43 expression is highly increased in both acute and chronic injuries, fostering inflammation and pro-apoptotic signaling [10–13]. Particularly, evidences showed that inhibition of Cx43-based channels reduces secondary damages during acute and chronic disorders [14, 15]. As such, Cx43 up-regulation in spinal cord astrocytes is critical for the maintenance of late-phase neuropathic pain, but the specific role of Cx43 is still worthy of further investigation to find new therapies for chronic neuropathic conditions.

The opioid system exerts physiological inhibitory effects on pain by activation of μ (MOR), δ (DOR), and k (KOR) opioid receptors [16, 17]. Despite their undeniable benefit for treating severe acute pain, MOR agonists present limited effectiveness for chronic pain therapy and relevant side effects such as constipation and tolerance development [18, 19]. DOR agonists, on the other side, showed a relevant preclinical efficacy in animal models of thermal and mechanical allodynia [20]. Interestingly, during chronic pain, DOR targeting to the cell surface was abolished in MOR-KO mice, suggesting that activation of MOR plays a crucial role in the regulation of DOR trafficking. A novel approach in drug discovery processes for pain is to develop safe and effective multitarget ligands, to enhance therapeutic profile [21]. In particular, MOR and DOR simultaneous targeting led to a better pharmacological fingerprint [22, 23]. Co-expression of DOR and MOR in key sites for pain modulation could be the cellular basis for their intermodulatory interactions [24]. We previously reported that benzomorphan-based compound LP2 is able to bind and to activate simultaneously MOR (K_i = 1.08 nM, IC_{50} = 21.5 nM) and DOR (K_i = 6.6 nM, IC_{50} = 4.4 nM) [25]. Moreover, LP2 was found to produce a significant anti-nociceptive (ED_{50} = 0.9 mg/kg i.p.) and anti-inflammatory effect (ED_{50} = 0.88 and 0.79 mg/kg i.p., in phases I and II of formalin test) [26], showing the pharmacodynamic profile of a potent multitarget MOR/DOR anti-nociceptive ligand [27].

Herein, we aimed to investigate the potential of simultaneous MOR/DOR targeting in a model of unilateral sciatic nerve chronic constriction injury (CCI). Moreover, the effects of LP2 treatment in the spinal cord cell populations of ipsi- and contra-lateral dorsal horns were evaluated during the time course of neuropathic pain. Thus, we analyzed the level of astrocytic Cx43 in the dorsal horns of CCI rats and its involvement in chronicization of neuropathy, to study the effects of LP2-induced opioidergic stimulation on glial activation and central sensitization.

Materials and Methods

Animal Models of Neuropathic Pain

Experiments were performed on male Sprague-Dawley rats (Harlan Laboratories) weighing 180–200 g. Animals were kept at a constant temperature (23–25 °C) under a 12/12-h light/dark cycle with free access to food and water. All tests were conducted at constant temperature (23–25 °C) between 9:00 am and 15:00 pm. This study was performed in accordance with the European Communities Council directive and Italian regulations (EEC Council 2010/63/EU and Italian D.Lgs. no. 26/2014) and all efforts were made to replace, reduce, and refine the use of laboratory animals. A total number of 54 male rats were used in this study. The total number of animals per group was calculated before the experiments, using power analysis (significant value = 0.05, potency = 0.8, magnitude = 0.8).

The CCI model was used to induce neuropathic pain in rats and was established according to Bennett and Xie [28] with minor modifications [29]. Briefly, animals were anesthetized with isoflurane inhalation (4% induction, 2% maintenance) and an incision was made below the hipbone, parallel to the left common sciatic nerve. The sciatic nerve was exposed and four ligatures (4/0 chromic silk, Ethicon) were tied tightly around the nerve at the level of the mid-thigh and proximal to the trifurcation of the nerve at about 1 mm spacing, until a brief twitch in the respective hind limb was observed. For sham operation, the sciatic nerve was exposed, and no ligatures were applied. Rats were randomly assigned to the different groups: naïve (n = 9), sham-vehicle (n = 15), CCI-vehicle (n = 18), and CCI-LP2 (n = 12). After randomization, rats received a daily intraperitoneal (i.p.) injection of either vehicle or LP2 (0.9 mg/kg i.p.) starting at 11 days post-ligatures (dpl). Body weight and behavioral assessment of mechanical allodynia were examined at 0 (before surgery), 3, 5, 11, 16, and 21 dpl. The assessment of tactile allodynia was performed by measuring the withdrawal threshold (g) of the hind paw in response to a series of calibrated von Frey's filaments, as previously described [30]. Rats were placed in a testing chamber with a wire mesh bottom and allowed to acclimatize for 20 min. The ventral surface of the hind paw was mechanically stimulated from below with an ascending series of graded von Frey's filaments with bending forces ranging from 0.02 to 30 g. The paw withdrawal threshold was determined by the "up-down" method [31] of sequentially increasing and decreasing the stimulus strength and data are expressed as the mean withdrawal threshold (g) ± standard error of the mean (SEM) and mean area under the threshold curve (A.U.C.) ± SEM.

Ex Vivo Tissue Processing

At 11, 16, and 21 dpl, rats were anesthetized with an i.p. injection of ketamine 10 mg/mL and xylazine 1.17 mg/mL and transcardially perfused with 0.5 M EDTA (Sigma) in normal saline, followed by ice cold 4% paraformaldehyde (PFA) in PBS (pH = 7.4). Spinal cords and dorsal root ganglions (DRGs) were isolated and post-fixed in 4% PFA in PBS at 4 °C overnight. Tissue samples were then washed in PBS and cryo-protected in 30% sucrose in PBS at 4 °C for 3 days. Samples were embedded in optimum cutting temperature (OCT) medium and snap frozen in liquid nitrogen for cryo-sectioning. Frozen OCT blocks were cryo-sectioned using a cryostat (Reichert-Jung 2800) with a microtome blade (Pathocutter, Japan) and 20-μm-thick axial sections were collected. Sections were stored at − 80 °C until use.

Immunoblotting

The total protein content of the lumbar portions of spinal cords was extracted from a total of 10 axial sections. L3–L5 sections were detached from SuperFrost slides (Thermo Scientific), collected, and homogenized in 30 μL 1X RIPA lysis buffer (abcam), supplemented with a cocktail of protease inhibitors (Sigma). Samples were incubated at 95 °C for 20 min and at 4 °C for 10 min. After sonication (5 cycles/30 s), protein content was quantified using a Pierce BCA Protein Assay kit (Thermo Scientific). Protein samples containing an equal amount of proteins (50 μg) were electrophoresed on 4–20% SDS-PAGE gels and transferred to nitrocellulose membranes. Membranes were incubated for 1 h at room temperature (RT) with blocking buffer (5% non-fat dry milk in 0.1% tween-20 in PBS) and then overnight at 4 °C with primary antibodies diluted in blocking buffer. The following primary antibodies were used for immunoblotting: mouse monoclonal anti-glial fibrillary acidic protein (GFAP) (BD Biosciences Cat. No. 610566, RRID: AB_397916, 1:1000), rabbit polyclonal anti-Cx43 (Cell Signaling Technology Cat. No. 3512, RRID: AB_2294590, 1:1000), and mouse monoclonal anti-β-tubulin (Sigma-Aldrich Cat. No. T4026, RRID: AB_477577, 1:5000). Then, membranes were washed three times in 0.1% tween-20 in PBS and incubated for 1 h at RT with the appropriate secondary antibody: goat polyclonal anti-mouse HRP-conjugated (Jackson ImmunoResearch Labs Cat. No. 115-035-003, RRID: AB_10015289, 1:50,000) or goat polyclonal anti-rabbit HRP-conjugated (Jackson ImmunoResearch Labs Cat. No. 111-035-144, RRID: AB_2307391, 1:100,000). Proteins bands were detected with west dura extended duration HRP substrate (Thermo Scientific) according to the manufacturer's instructions and revealed with UVITEC Cambridge Imaging System.

The density of each band was quantified using ImageJ analysis software and band density was normalized to the β-tubulin optical density measured in the same membrane. All values are shown as the mean fold change (FC) over sham ± SEM.

Cell Cultures

DRG neurons were derived as previously described [32] with minor modifications. $N = 6$ naïve adult Sprague-Dawley rats were humanely culled and the vertebral columns were isolated and kept in dry iced L15 medium (Leibovitz). Lumbar L1–L5 DRGs were extracted and placed in a petri dish in dry iced L15 medium supplemented with 1x pen/strep. DRGs were collected and digested in collagenase (2 mg/mL) for 1 h at 37 °C and 5% CO_2. Then, tissues were digested in trypsin for 10 min at 37 °C and 5% CO_2. After enzymatic digestion, DRGs were mechanically triturated, loaded in 10 mL of 15% BSA in DMEM (4.5 g/L glucose) to remove debris and myelin, and centrifuged at $1000 \times g$ for 5 min. Cells were collected, suspended in DRG neuron medium [NGF 2 ng/mL, 1x GlutaMax, 1x pen/strep, FBS 1% in DMEM (4.5 g/l glucose)] and plated in Matrigel-coated 24-well plates (1×10^4 cells/well/400 μL). The day after, half of the medium was replaced with fresh DRG neuron medium and neurons were cultured for the following 7 days.

Astrocytes were derived as previously described [33], adapting the protocol to derive spinal astrocytes. Spinal cords from $n = 6$ naïve adult Sprague-Dawley rats were isolated and kept in dry iced L15 medium (Leibovitz). Tissues were dissected using iridectomy scissors in small pieces and mechanically triturated in astrocyte medium (1x pen/strep, FBS 20% in DMEM high glucose). Suspension was then filtered through a sterile nylon sieve (82 μm pore size) and fresh medium was added to adjust the cell density to 2.0×10^5 cells/mL. Cells were plated in a 24-well plate at a final density of 1.0×10^5 cells/well/500 μL and cultured for the following 20 days. Media were replaced every 4 days. All cell lines were cultured at 37 °C in a humidified atmosphere of 5% CO_2.

Conditioned Medium Experiments

On the day of the experiment, media were removed and fresh DRG neuron media supplemented with 100 μM picrotoxin were added to picrotoxin-stimulated cell cultures for 1 h. Control unstimulated cell cultures received fresh media with vehicle (PBS). After stimulation media were removed, cell cultures were washed in PBS and fresh DRG neuron media with vehicle were added to control and picrotoxin cultures and 1 μM LP2 was added to picrotoxin+LP2 cultures for 24 h. Conditioned media from DRG neurons were collected after 24 h, filtered using 0.22 μm mesh filters, and kept at − 80 °C until use. Media were added to astrocytes plated in 24-well plates and cultured for 24 h for qRT-PCR and immunofluorescence analysis.

LDH Activity Assay

The toxicity of picrotoxin and LP2 treatment was ascertained using a lactate dehydrogenase (LDH) activity assay (CytoSelect™ LDH Cytotoxicity Assay Kit, Cell Biolabs) following the manufacturer's instructions. We used 10% Triton X-100 in PBS-treated cells as the positive control (100% toxicity) and untreated live cells as the negative control (0% toxicity). The percentage of relative cytotoxicity for experimental samples was calculated as: $[(OD_{sample} - OD_{negative\ control}) / (OD_{positive\ control} - OD_{negative\ control})] \times 100$. Assays were performed on the media of DRG-derived neurons grown in 24-well plates for 24 h post-picrotoxin stimulations or 24 h post-LP2 treatment.

qRT-PCR

For qRT-PCR analysis, equal amounts of RNA were reverse-transcribed using the High Capacity cDNA Reverse Transcription Kit (ThermoFisher Scientific) according to the manufacturer's instructions. cDNA was then quantified with the NanoDrop 2000c instrument (ThermoFisher Scientific) and qRT-PCR was performed with the PowerUp SYBR Green Master Mix (ThermoFisher Scientific). Rat-specific primers were designed for Gfap, Gap junction alpha-1 protein (Gja1), solute carrier family 1 member 2 (Slc1a2), solute carrier family 1 member 3 (Slc1a3), and Actb (used as housekeeping gene), and the primer sequences were confirmed by BLAST analysis for highly similar sequences against known databases and tested for specificity (Table 1).

All samples were tested in triplicate on a 7900HT Fast Real-Time PCR System (ThermoFisher Scientific) and analyzed using the $2^{-\Delta\Delta CT}$ method.

Immunofluorescence and Quantifications

For quantification of the percentage of cleaved caspase 3 (Cl Casp3)-positive cells and Cl Casp3-NeuN double-positive cells, sections were washed in PBS and blocked in immunofluorescence blocking buffer [10% normal goat serum (NGS) and 0.1% Triton X-100 in PBS] for 1 h at RT. Sections were then incubated overnight at 4 °C with rabbit polyclonal anti-Cl Casp3 (Cell Signaling Technology Cat. No. 9661S, RRID: AB_2341188, 1:500) and mouse monoclonal (A60) anti-NeuN (Millipore Cat. No. MAB377, RRID: AB_2298772, 1:100) antibody. On the following day, sections were washed in 0.1% Triton X-100 in PBS three times at RT and then incubated 1 h at RT with appropriate secondary antibody: goat polyclonal anti-mouse (Alexa Fluor 488, Thermo Fisher Scientific Cat. No. A-11001, RRID: AB_2534069, 1:1000 or Alexa Fluor 546, Innovative Research Cat. No. A21045, RRID: AB_1500928, 1:1000) and goat polyclonal anti-rabbit (Alexa Fluor 488, Molecular Probes Cat. No. A-11008, RRID: AB_143165, 1:1000 or Alexa Fluor 564, Molecular Probes Cat. No. A-11010, RRID: AB_143156, 1:1000). Sections were then washed in 0.1% Triton X-100 in PBS three times at RT, and nuclei were counterstained with DAPI (1:10,000, Invitrogen) for 5 min at RT and then mounted with BrightMount mounting medium (abcam). Nonspecific staining was observed in control incubations in which the primary antibodies were omitted. Quantification of the percentage of positive cells was obtained quantifying the number of Cl Casp3-positive nuclei or Cl Casp3 and NeuN double-positive nuclei from randomized regions of interest (ROI) of $n = 3$ dorsal horns in L2–L5 tract of the spinal cord of $n = 3$ rats/group. Percentages were obtained counting $n \geq 300$ nuclei per ROI. Data are shown as mean percentage of positive cells over total DAPI-positive cells or over NeuN-positive cells ± SEM.

For in vitro immunofluorescence analysis on neurons and astrocytes, at the end of the experiment, cultures were washed in PBS and fixed with 4% PFA 10 min at RT.

For GFAP, Cx43, MOR, and DOR immunofluorescence analysis, ex vivo sections or in vitro cultures were washed in PBS and blocked in immunofluorescence blocking buffer for 1 h at RT. Samples were then incubated overnight at 4 °C with mouse monoclonal anti-GFAP (BD Biosciences Cat. No. 610566, RRID: AB_397916, 1:500), rabbit polyclonal anti-Cx43 (Cell Signaling Technology Cat. No. 3512, RRID: AB_2294590, 1:200), rabbit polyclonal anti-MOR (Merck Millipore Cat. No. AB1580-I, RRID: AB_2716850, 1:1000), rabbit polyclonal anti-DOR (Merck Millipore Cat. No. AB1560, RRID: AB_90778, 1:1000), or rabbit monoclonal anti-phospho

Table 1 Oligonucleotide sequence of primers used in qRT-PCR

Target	Forward	Reverse
	Primer sequences	
Gfap	5′-TCA TGG ACG GCA CAG ACC AC-3′	5′-GCC TGC CAC ATG CCA AGA A-3′
Gja1	5′-GAA AGA GAG GTG CCC AGA C-3′	5′-GCC AGG TTG TTG AGT GTT AC-3′
Slc1a2	5′-AGT ATG TGG CGG CTG CT TC-3′	5′-GGA AAT GAT GAG AGG GAG GAT GAG-3′
Slc1a3	5′-AGC AGA GGA GGC TCC AAA GGG-3′	5′-CCA GAA GAG GAT GCC CAG AGG-3′
Actb	5′-ATC CCA TCA CCA TCT TCC AG-3′	5′-ATG AGT GTC CTT CCA CGA TAC CA-3′

(P)-Stat 3 (Cell Signaling Technology Cat. No. 9145, RRID:AB_2491009, 1:1000). On the following day, sections were washed in 0.1% Triton X-100 in PBS three times at RT and then incubated 1 h at RT with appropriate anti-mouse and anti-rabbit secondary antibody: goat polyclonal anti-mouse (Alexa Fluor 488, Thermo Fisher Scientific Cat. No. A-11001, RRID: AB_2534069, 1:1000 or Alexa Fluor 546, Innovative Research Cat. No. A21045, RRID: AB_1500928, 1:1000) and goat polyclonal anti-rabbit (Alexa Fluor 488, Molecular Probes Cat. No. A-11008, RRID: AB_143165, 1:1000 or Alexa Fluor 564, Molecular Probes Cat. No. A-11010, RRID: AB_143156, 1:1000). Sections and in vitro cell cultures were then washed in 0.1% Triton X-100 in PBS three times at RT, and nuclei were counterstained with DAPI (1:10,000, Invitrogen) for 5 min at RT and then mounted with BrightMount mounting medium (abcam). Nonspecific staining was observed in control incubations in which the primary antibodies were omitted. Quantification of the fluorescence intensity was performed by applying iso-data threshold on dorsal horn immunofluorescence images of $n = 4$ equally spaced sections of L2–L5 tract of the spinal cord or on the entire section of isolated DRGs of $n = 4$ rats/group. Data were normalized on the total area and expressed as mean FC over sham or sham-vehicle ± SEM. For P-Stat3, astrocyte soma was segmented and the corresponding P-Stat3 fluorescence intensity quantified using ImageJ analysis software. The percentage of cells with high P-Stat3 expression was obtained by dividing the number of cells with value over a fixed threshold for the total number of cells. Data are shown as mean percentage ± SEM. Investigators blinded to the treatment groups performed all quantifications.

For neuron-specific class III beta-tubulin (TUJ1) staining, cultures were washed in PBS and blocked in immunofluorescence blocking buffer for 1 h at RT. Samples were then incubated overnight at 4 °C with mouse monoclonal anti-TUJ1 (BioLegend Cat. No. 801201, RRID: AB_2313773, 1:200). On the following day, cultures were washed in 0.1% Triton X-100 in PBS three times at RT and then incubated 1 h at RT with anti-rabbit secondary antibody: goat polyclonal anti-mouse (Alexa Fluor 488, Thermo Fisher Scientific Cat. No. A-11001, RRID: AB_2534069, 1:1000). Nonspecific staining was observed in control incubations in which the primary antibodies were omitted. Quantification of the fluorescence intensity was performed by applying iso-data threshold on immunofluorescence images of $n = 3$ ROIs from $n = 6$ cultures from $n = 6$ naïve rats/group. Data were normalized on the total area and expressed as mean FC over sham or sham-vehicle ± SEM. Neurites were measured from $n = 6$ cultures from $n = 6$ naïve rats/group. Data are expressed as violin plot of neurites lengths expressed in micrometer. Investigators blinded to the treatment groups performed all quantifications.

Experimental Design and Statistical Analysis

All tests were performed in GraphPad Prism (version 5.00 for Mac, GraphPad Software) or RStudio (version 1.0.153, RStudio Inc.). Data were tested for normality using a D'Agostino and Pearson omnibus normality test and subsequently assessed for homogeneity of variance. Data that passed both tests were further analyzed by two-tailed unpaired Student's t test for comparison of $n = 2$ groups. Comparisons of $n > 2$ groups were performed using a one-way ANOVA and Holm-Sidak's multiple comparisons test. Statistical analyses of behavioral assessment of mechanical allodynia were performed using a two-way ANOVA repeated measure and Holm-Sidak's multiple comparisons test. For two-tailed unpaired Student's t tests, Welch-corrected t values (t) and degrees of freedom (df) are reported. For ANOVA tests, F values for groups, treatments, timepoints, or interactions are expressed as $F_{\text{comparison}}(\text{dfn},\text{dfd})$, where degrees of freedom numerator (dfn) $= a - 1$ and degrees of freedom denominator (dfd) $= N - a$, where a = number of groups and N = total number of subjects in the experiment. Principal component analysis (PCA) and cluster dendrogram were made in RStudio using fluorescence intensity data (for astrocytic GFAP and Cx43) and mRNA level data (for astrocytic *Gfap*, *Gja1*, *Slc1a2*, and *Slc1a3*). For all statistical tests, p values < 0.05 were considered statistically significant.

Results

CCI Rats Show Reactive Astrogliosis and Cx43 Up-Regulation in Ipsi-Lateral Dorsal Horn

To investigate the pathophysiological features of chronic pain, we established an in vivo model of neuropathy, CCI, by applying four ligatures in the left sciatic nerve (Fig. 1A).

Time course analysis of mechanical allodynia development upon ligature application showed that CCI rats had reduced withdrawal threshold starting from 3 dpl with a robust decrease at 11 dpl (2.0 ± 0.5 g CCI vs. 11.0 ± 2.1 g sham, $F_{\text{groups}}(1, 7) = 38.32$; $F_{\text{dpl}}(3, 21) = 3.339$; $F_{\text{groups} \times \text{dpl}}(3, 21) = 7.443$; Fig. 1B). The results were also expressed as total area under the withdrawal threshold curve, and we found a significant decrease of the total A.U.C. in CCI rats compared to sham-operated controls (52.32 ± 6.7 CCI vs. 133.7 ± 2.2 sham, $t = 11.61$, $df = 5.946$; Fig. 1C).

We then analyzed the spinal cord of sham and CCI rats at 11 dpl. Quantification of the total number of Cl Casp3-positive nuclei showed a significant increase of the proportion of suffering cells in the ipsi-lateral dorsal horn of CCI rats ($5.0 \pm 0.6\%$ CCI vs. $2.9 \pm 0.5\%$ sham, $t = 2.792$, $df = 3.982$; Fig. 1D, E). In order to find whether this pro-apoptotic phenotype was also related to neuronal distress,
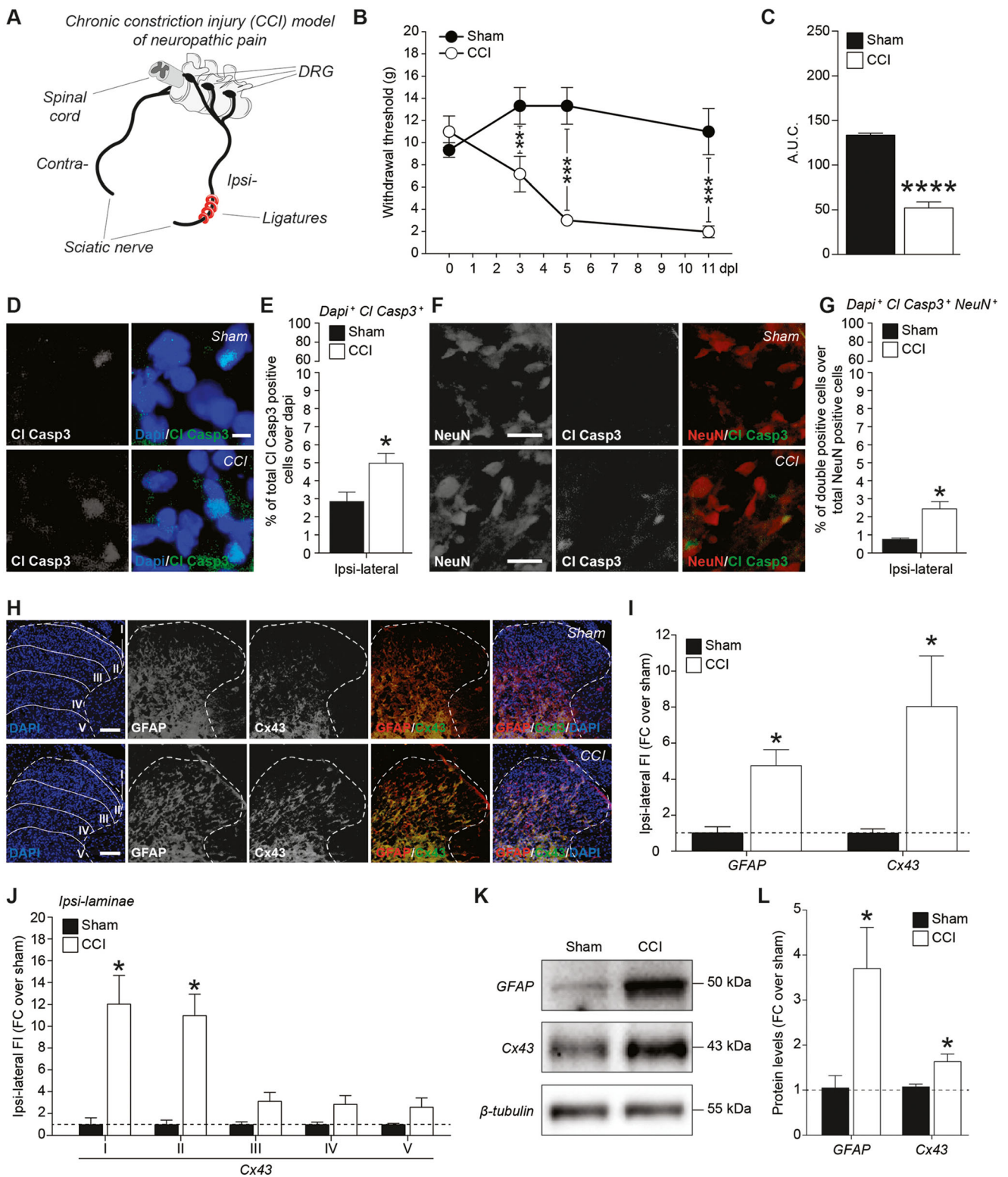
the fraction of Cl Casp3 and NeuN double-positive cells was further quantified. Our data suggested that a significant proportion of Cl Casp3-positive cells were NeuN-positive neurons located in the ipsi-lateral dorsal horn of the spinal cord of CCI rats ($2.4 \pm 0.4\%$ CCI vs. $0.7 \pm 0.1\%$ sham, $t = 4.106$, $df = 2.132$; Fig. 1F, G). No statistically significant differences were found in the contra-lateral total cell populations of Cl Casp3-positive cells and in the proportion of NeuN-Cl Casp3 double-positive cells (Fig. S1).

◄ **Fig. 1** CCI rats show reactive astrogliosis and Cx43 up-regulation in ipsi-lateral dorsal horns. **A** CCI model of neuropathic pain induced by application of four ligatures into the left (ipsi-lateral) sciatic nerve. **B** Withdrawal thresholds measured with von Frey's filaments on sham-operated and CCI rats at 0, 3, 5, and 11 dpl. Data are shown as mean ± SEM of $n = 3$ sham and $n = 6$ CCI rats. **C** Quantification of the area under the withdrawal threshold curve (A.U.C.) showed in **B** of sham and CCI rats. Data are shown as mean ± SEM of $n = 3$ sham and $n = 6$ CCI rats. **D**, **E** Representative images of Cl Casp3 immunofluorescence analysis (**D**) and quantification (**E**) of the percentage of total Cl Casp3 and DAPI double-positive cells over DAPI in the ipsi-lateral dorsal horns. Data are shown as mean ± SEM of $n = 3$ rats per group. Scale bars = 5 μm. **F**, **G** Representative images of Cl Casp3 and NeuN immunofluorescence analysis (**F**) and quantification (**G**) of the percentage of Cl Casp3 and NeuN double-positive cells over total NeuN-positive cells in the ipsi-lateral dorsal horns. Data are shown as mean ± SEM of $n = 3$ rats per group. Scale bars = 10 μm. **H**, **I** Representative pictures of GFAP and Cx43 immunofluorescence analysis (**H**) and quantification (**I**) of GFAP and Cx43 fluorescence intensity of the ipsi-lateral dorsal horns of sham-operated and CCI rats at 11 dpl. Data are shown as FC over sham ± SEM of $n = 4$ rats per group. Scale bars = 100 μm. **J** Quantification of Cx43 fluorescence intensity of ipsi-lateral *laminae* I–V of sham and CCI rats at 11 dpl. Data are shown as mean FC over sham ± SEM of $n = 4$ rats per group. **K**, **L** Representative blots (**K**) and quantification (**L**) of GFAP and Cx43 protein levels in the lumbar region of the spinal cords of sham and CCI rats at 11 dpl. Data are shown as mean FC over sham ± SEM of $n = 4$ rats per group. DRG, dorsal root ganglion; Dpl, days post-ligatures; A.U.C., area under curve; Cl Casp3, cleaved caspase 3; FI, fluorescence intensity; FC, fold change. *p value < 0.05, **p value < 0.01, ***p value < 0.001, and ****p value < 0.0001 CCI vs. sham

We next hypothesized that increased pro-apoptotic signaling in ipsi-lateral dorsal *laminae* may exert pro-gliosis effects on spinal cord astrocytes in ipsi-lateral dorsal horn. We found that CCI rats exhibit a significant increase of GFAP in the ipsi-lateral *laminae* and a remarkable intensification of Cx43 levels (8.0 ± 2.8-fold increase vs. sham, $t = 3.903$, $df = 3.869$; Fig. 1H, I). Of note, Cx43 fluorescence intensity was increased in ipsi-lateral *lamina* I and *lamina* II of CCI rats compared to sham rats, although no significant differences were detected in *laminae* III–V (Fig. 1J). No significant differences were found in GFAP and Cx43 fluorescence intensity in contra-lateral dorsal horn (Fig. S1).

To confirm these findings, we then analyzed the level of GFAP and Cx43 on total protein content of lumbar spinal cord of sham-operated and CCI rats, detecting a significant increase of GFAP (3.7 ± 0.9-fold increase vs. sham, $t = 2.774$, $df = 3.542$), as index of underlying astrogliosis, as well as increased levels of Cx43 as main astrocytic connexin (~ 2-fold increased vs. sham, $t = 3.176$, $df = 3.852$; Fig. 1K, L).

Altogether, our findings suggest that chronic pain induces a pro-apoptotic signaling in the CNS of CCI rats with a reactive astrogliosis fostered by Cx43 up-regulation in ipsi-lateral dorsal horn.
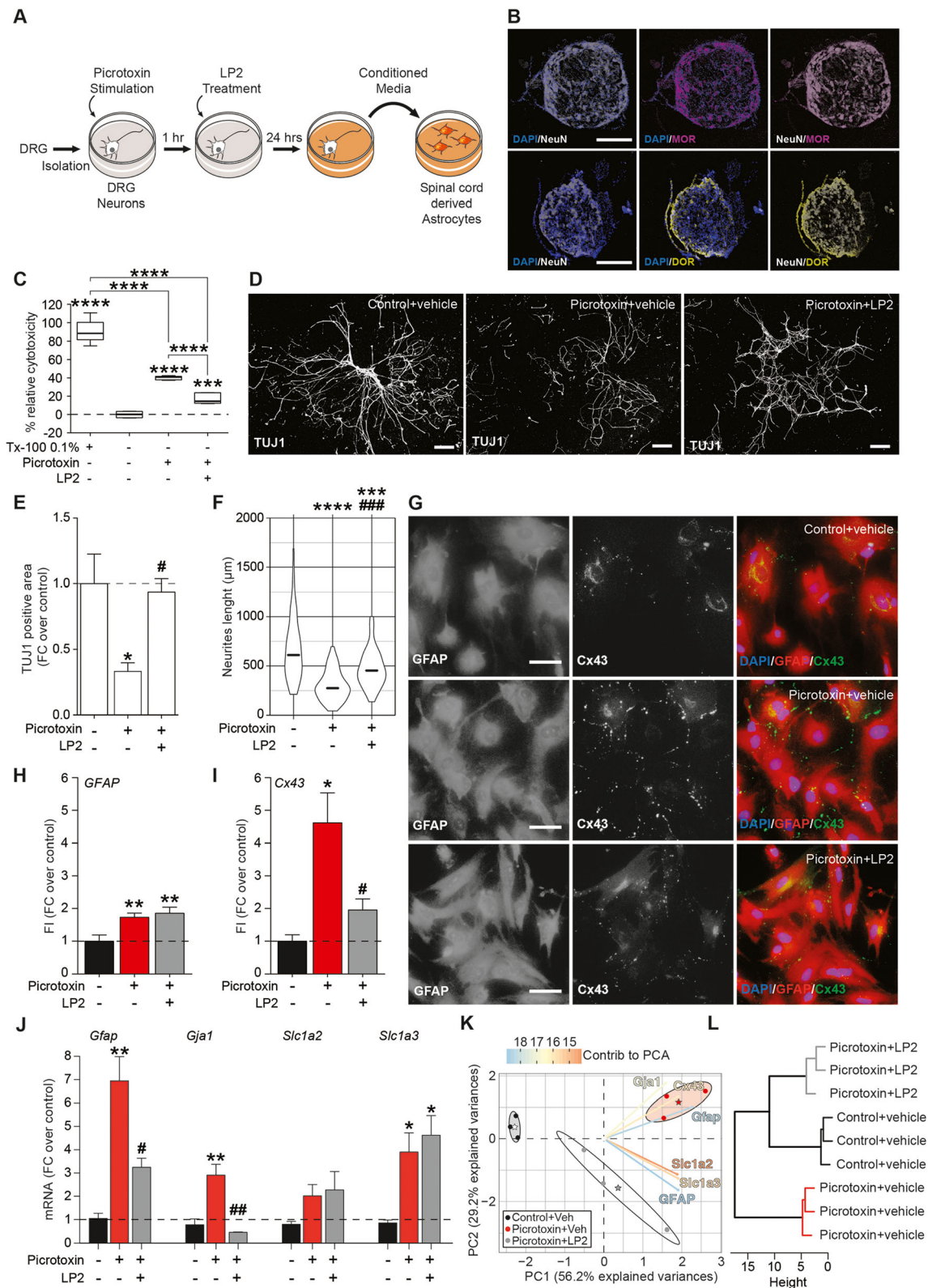
Dorsal Root Ganglion Neurons Excitotoxic Conditioned Medium Induces Up-Regulation of GFAP and Cx43 in Spinal Cord-Derived Astrocytes In Vitro

Neuronal influence on spinal cord-derived astrocyte phenotype was investigated in vitro in an experimental model of excitotoxicity and the effects of LP2 as a MOR/DOR targeting molecules were analyzed in this model (Fig. 2A). Expression analysis of MOR and DOR in DRGs isolated from naïve rats reveals a strong co-localization between NeuN-positive neurons and both MOR and DOR (Fig. 2B). As such, we used primary DRG-derived neurons as conditioning cell lines and LP2-responsive cells in our in vitro setting. Firstly, neurons were treated with increasing concentration of LP2, showing that 1 μM LP2 concentration does not affect neurons viability (Fig. S2). Then, DRG neurons were exposed to 1 h stimulation with picrotoxin in order to induce excitotoxic pulse; thus, media were removed and medium plus vehicle or medium plus LP2 treatment was added for 24 h. We found that 1-h picrotoxin increased the relative cytotoxicity in DRG neurons and that LP2 treatment was able to significantly prevent these neurotoxic effects exerting, at least partially, a neuroprotective effect towards excitotoxic pulse (Fig. 2C). The effects of picrotoxin-induced excitotoxicity on DRG neurons were analyzed and we found a significant reduction of the TUJ1-positive area (0.33 ± 0.07 picrotoxin + vehicle, FC over control + vehicle, $F_{treatment}(2, 15) = 6.300$; Fig. 2D, E) and neurite length in picrotoxin-stimulated neurons (Fig. 2F). LP2 was able to revert these neurodegenerative phenomena promoting a protective effect on the overall sprouting of DRG neurons (0.94 ± 0.10 picrotoxin+LP2, FC over control + vehicle, $F_{treatment}(2148) = 34.07$) and maintaining a significant increased neurite length compared to picrotoxin-stimulated untreated cultures (Fig. 2D–F).

We then moved to analyze the effects of neuron-conditioned media on primary spinal cord-derived astrocyte cultures. Firstly, we detected a significant increase in GFAP fluorescence intensity and a tight Cx43-mediated cell coupling in astrocytes treated with conditioned media from picrotoxin-stimulated neurons (Fig. 2G–I). Conditioned media from stimulated DRG neurons treated with LP2 did not significantly affect GFAP intensity (Fig. 2H), although we found a significant reduction of the Cx43-mediated cell coupling at 24 h (1.9 ± 0.3 picrotoxin + LP2 vs. 4.6 ± 0.9 picrotoxin + vehicle, FC over control + vehicle, $F_{treatment}(2, 23) = 7.597$; Fig. 2I). This effect was coupled with a significant increase of P-Stat 3 nuclear intensity in astrocytes exposed to conditioned media from picrotoxin-stimulated neurons, effects not detected in astroglial cultures treated with conditioned media collected from picrotoxin-stimulated LP2-treated neuronal cultures (Fig. S3).

Finally, Gfap, Gja1, Slc1a2, and Slc1a3 mRNA levels were evaluated in spinal cord-derived astrocytes treated with

conditioned media from control-vehicle, stimulated with picrotoxin plus vehicle and stimulated with picrotoxin treated with LP2 neurons. We found that picrotoxin stimulation induced a significant increase of Gfap mRNA levels that was

reverted by LP2 treatment on DRG neurons (Fig. 2J). A significant increase of Gja1 levels was also detected upon picrotoxin stimulation and was abolished by LP2 treatment after DRG neuron picrotoxin stimulation. We also analyzed

◀ **Fig. 2** DRG excitotoxic conditioned medium induces up-regulation of GFAP and Cx43 in spinal cord-derived astrocytes in vitro. **A** Experimental paradigm spinal cord-derived astrocytes treated with DRG neurons conditioned media. **B** Representative images of MOR- and DOR-positive NeuN-positive neurons in DRG isolated from naïve rats. Scale bars = 100 μm. **C** LDH activity assay in DRG neuron-positive and neuron-negative controls, DRG neurons stimulated with picrotoxin treated with vehicle and stimulated with picrotoxin treated with LP2. Data are shown as standard box-and-whisker plot, in which the central line represents the median and the upper and lower bounds are min and max value. Data are shown as mean percentage of controls of $n = 3$ independent experiments from $n = 6$ naïve rats. **D–F** Representative pictures (**D**) and quantification of TUJ1-positive area (**E**) and neurite length (**F**) of TUJ1-positive DRG neuron control + vehicle, picrotoxin + vehicle, and picrotoxin treated with LP2. Data in **E** are shown as mean FC over control + vehicle ± SEM of $n = 3$ independent experiments from $n = 6$ naïve rats. Data in **F** are shown as violin plot of $n > 40$ neurites/group. **G–I** Representative pictures of GFAP and Cx43 immunofluorescence analysis (**G**) and quantifications of GFAP (**H**) and Cx43 (**I**) fluorescence intensity in spinal cord-derived astrocytes treated with control + vehicle, picrotoxin + vehicle, and picrotoxin+LP2 DRG neuron-conditioned media. Data are shown as mean FC over control + vehicle ± SEM of $n = 3$ independent experiments from $n = 6$ naïve rats. Scale bars = 30 μm. **J** qRT-PCR for Gfap, Gja1, Slc1a2, and Slc1a3 levels on spinal cord-derived astrocytes treated with control, stimulated with picrotoxin, and stimulated with picrotoxin treated with LP2 DRG neuron-conditioned media. Data are shown as mean FC over control + vehicle ± SEM of $n = 3$ independent experiments from $n = 6$ naïve rats. **K** Principal component analysis (PCA) and ellipses of confidence of GFAP and Cx43 immunofluorescence and *Gfap, Gja1, Slc1a2,* and *Slc1a3* mRNA levels for astrocytes treated with DRG-conditioned media (control + vehicle vs. picrotoxin + vehicle vs. picrotoxin + LP2). Stars represent the mean points for each ellipse. Colors of variable arrows are function of the contribution to the PCA. **L** Cluster dendrogram of PCA in **K**. DRG, dorsal root ganglion; Tx-100, Triton X-100; FC, fold change; FI, fluorescence intensity; PC, principal component. $*p$ value < 0.05, $**p$ value < 0.01, $***p$ value < 0.001, and $****p$ value < 0.0001 vs. control + vehicle or between indicated groups. $^{\#}p$ value < 0.05, $^{\#\#}p$ value < 0.01, and $^{\#\#\#}p$ value < 0.001 vs. picrotoxin + vehicle

glutamate transporter genes in primary astrocytes, finding not significant modulation of Slc1a2 mRNA levels encoding for glutamate transporter 1 (GLT-1) and a significant increase of Slc1a3 mRNA levels encoding for glutamate aspartate transporter (GLAST). Both these mRNAs were not modulated by LP2 treatment on DRG neurons (Fig. 2J). Hence, to assess the multivariate effects of astroglial responses to neuronal conditioned media, we integrated these data using a PCA for GFAP and Cx43 fluorescence intensity and for mRNA level data. We integrate our data generating principal components, founding that PC1 and PC2 explain a total of 85.4% of the variation (Fig. 2K). We found that astrocytes exposed to media from picrotoxin + vehicle treated neurons differentially clusterized compared to control + vehicle (Fig. 2K, L) and that astrocytes exposed to conditioned media from picrotoxin + LP2-treated neurons were found to cluster closer to unstimulated controls (Fig. 2K, L).

These data suggest that over-stimulated neurons exposed to excitotoxic stimuli significantly modified astrocyte phenotype and that LP2 treatment exerts neuroprotective effects by

preventing astroglial activation and Cx43 increase. This evidence prompted us to further investigate the effects of MOR/ DOR targeting in vivo on spinal cord in CCI rats.

MOR and DOR Targeting by LP2 Ameliorates Mechanical Allodynia in CCI Rats

In order to find a potential effect of MOR/DOR multitarget ligand LP2 in vivo, immunofluorescence analysis was performed to examine the localization of these receptors in the spinal cord of naïve rats, confirming that *lamina* I and II cell populations showed high levels of MORs and DORs in the spinal cord (Fig. 3A, B). Thus, the effects of LP2 in mediating ameliorating effects on CCI rats during the allodynia time course were evaluated (Fig. 3C). Notably, simultaneous MOR/DOR targeting significantly increased the withdrawal threshold of CCI rats as compared to CCI-vehicle rats at 16 dpl (7.0 ± 0.6 g CCI-LP2 vs. 0.65 ± 0.1 g CCI-vehicle) and 21 dpl (6.5 ± 0.5 g CCI-LP2 vs. 0.85 ± 0.2 g CCI-vehicle, $F_{\text{groups}}(2, 36) = 28.06$; $F_{\text{dpl}}(3, 36) = 14.28$; $F_{\text{groups} \times \text{dpl}}(6, 36) = 4.509$; Fig. 3D), coupled with a significant increase of the overall A.U.C. of the withdrawal threshold curve (96.1 ± 7.7 CCI-LP2 vs. 50.5 ± 13.9 CCI-vehicle, $F_{\text{groups}}(2, 9) = 24.09$; Fig. 3E).

We next asked whether LP2-induced behavioral amelioration was paired with spinal cord astrocyte modulation. As shown in Fig. 4, we detected a robust GFAP and Cx43 increase in CCI-vehicle rats compared to sham-vehicle rats also at 16 dpl and at 21 dpl (Fig. 4A–C). LP2 treatment effectively reduced GFAP at 21 dpl (2.3 ± 0.7 CCI-LP2 vs. 5.5 ± 0.8 CCI-vehicle, FC over sham-vehicle $F_{\text{treatment}}(2, 9) = 13.27$) with no significant modifications of GFAP fluorescence intensity at 16 dpl compared to CCI-vehicle rats (p value = 0.7286 CCI-LP2 vs. CCI-vehicle). Notably, LP2 treatment significantly reduced Cx43 at 16 dpl (1.9 ± 0.5 CCI-LP2 vs. 6.7 ± 1.9 CCI-vehicle, FC over sham-vehicle, $F_{\text{treatment}}(2, 9) = 7.312$) and at 21 dpl ($1.2 \pm 0.4$ CCI-LP2 vs. 5.2 ± 0.8 CCI-vehicle, FC over sham-vehicle, $F_{\text{treatment}}(2, 9) = 22.27$) in the ipsilateral dorsal horns as compared to CCI-vehicle-treated rats (Fig. 4C).

We next evaluated the fluorescence intensity of Cx43 in ipsi-lateral *laminae* I–V founding a not significant reduction of Cx43 levels in CCI-LP2 *lamina* I at 16 dpl compared to CCI-vehicle rats, significantly reduced in CCI-LP2 at 21 dpl (1.3 ± 0.3 CCI-LP2 vs. 8.1 ± 1.9 CCI-vehicle, FC over sham-vehicle, $F_{\text{treatment}}(2, 9) = 12.73$; Fig. 4D). Cx43 fluorescence intensity was significantly reduced in *lamina* II in CCI-LP2 rats at 16 dpl compared to CCI-vehicle and not significantly increased compared to sham-vehicle group at 21 dpl (Fig. 4D). No significant differences were detected in Cx43 fluorescence intensity in *laminae* III, IV, and V at 16 dpl (Fig. 4D).
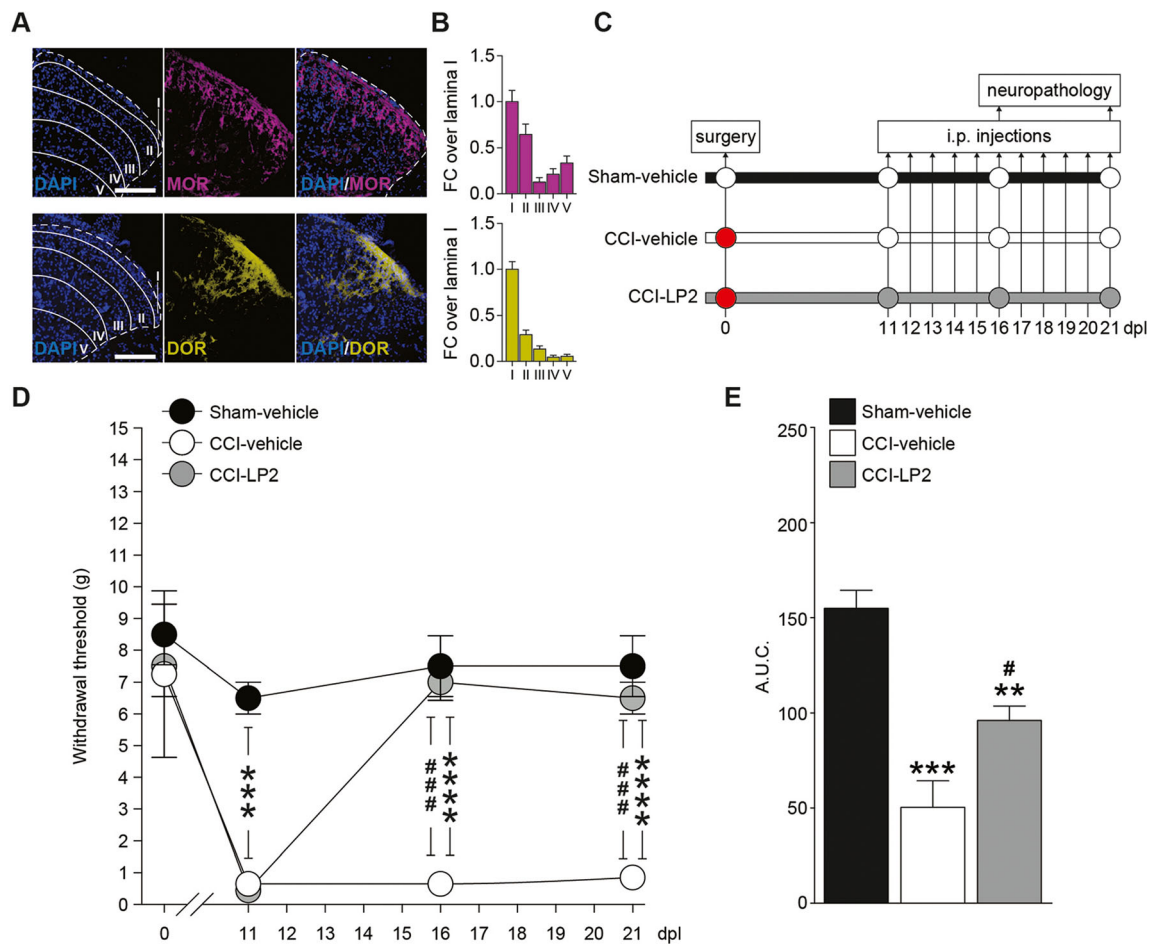
Fig. 3 MOR and DOR targeting by LP2 ameliorates mechanical allodynia in CCI rats. **A, B** Representative images (**A**) and quantification (**B**) of MOR and DOR in *laminae* I–V of the spinal cord dorsal horns of naïve rats. Scale bars = 100 μm; data are shown as mean FC over *lamina* I ± SEM of $n = 3$ naïve rats. **C** Experimental paradigm of CCI induction and LP2 treatment of CCI rats. **D** Withdrawal thresholds measured with von Frey's filaments on sham-vehicle, CCI-vehicle rats, and CCI-LP2-treated rats at 0, 11, 16, and 21 dpl. Data are shown as mean ± SEM of $n = 4$ rats per group. **E** Quantification of the area under the withdrawal thresholds curve (A.U.C.) showed in **E** of sham-vehicle, CCI-vehicle, and CCI-LP2-treated rats. Data are shown as mean area ± SEM of $n = 4$ rats per group. A.U.C., area under curve; dpl, days post-ligatures; i.p., intraperitoneal injection; FC, fold change. **p value < 0.01, ***p value < 0.001, and ****p value < 0.0001 vs. sham-vehicle. #p value < 0.05, ##p value < 0.01, and ###p value < 0.001 vs. CCI-vehicle

LP2 effects on contra-lateral dorsal horn astrocyte population and Cx43 levels were also analyzed. On one hand, we found a significant increase of the total dorsal horn GFAP immunofluorescence at 16 dpl in CCI-vehicle rats and CCI-LP2 rats, which was restored to control levels at 21 dpl by LP2 treatment. On the other hand, we did not detect any significant difference in Cx43 immunofluorescence at both 16 dpl ($F_{treatment}(2, 9) = 0.5943$) and 21 dpl ($F_{treatment}(2, 9) = 4.162$) between groups (Fig. S4). We finally analyzed Cx43 fluorescence intensity in contra-lateral dorsal horn *laminae* I–V founding no significant difference at 16 and 21 dpl (Fig. S4).

LP2 Reduces Astrocytic Cx43 in Ipsi-Lateral Dorsal Horns of CCI Rats

To determine Cx43 expression profile in spinal dorsal horn during ongoing neuropathy, immunofluorescence analysis on spinal cord sections was performed. We found reactive Cx43 activation in ipsi-lateral dorsal horn of CCI-vehicle rats with high Cx43-GFAP co-localization profile compared to sham-vehicle rats (Fig. 5A−A″, B−B″). LP2-treated CCI rats showed a reduced site-specific localization of Cx43 as compared to CCI-vehicle rats (Fig. 5C–C″). The profile plot of GFAP and Cx43 showed a strong juxtaposition between GFAP peaks and Cx43 peaks (Fig. 5D–F). By analyzing the levels of GFAP and Cx43 at 16 and 21 dpl in the lumbar portion of the spinal cord of sham-vehicle rats, CCI-vehicle rats, and CCI-LP2 treated rats, we confirmed that CCI induces GFAP with an increase (~ 2-fold) at 16 dpl, significantly reverted by LP2 treatment at 21 dpl (0.6 ± 0.1 CCI-LP2 vs. 2.4 ± 0.5 CCI-vehicle, FC over sham-vehicle, $F_{treatment}(2, 6) = 8.423$; Fig. 5G, H). Consistent with the immunofluorescence analysis, Cx43 was not significantly higher in CCI-LP2 rats as compared to sham-vehicle controls at 16 dpl (*p* value =
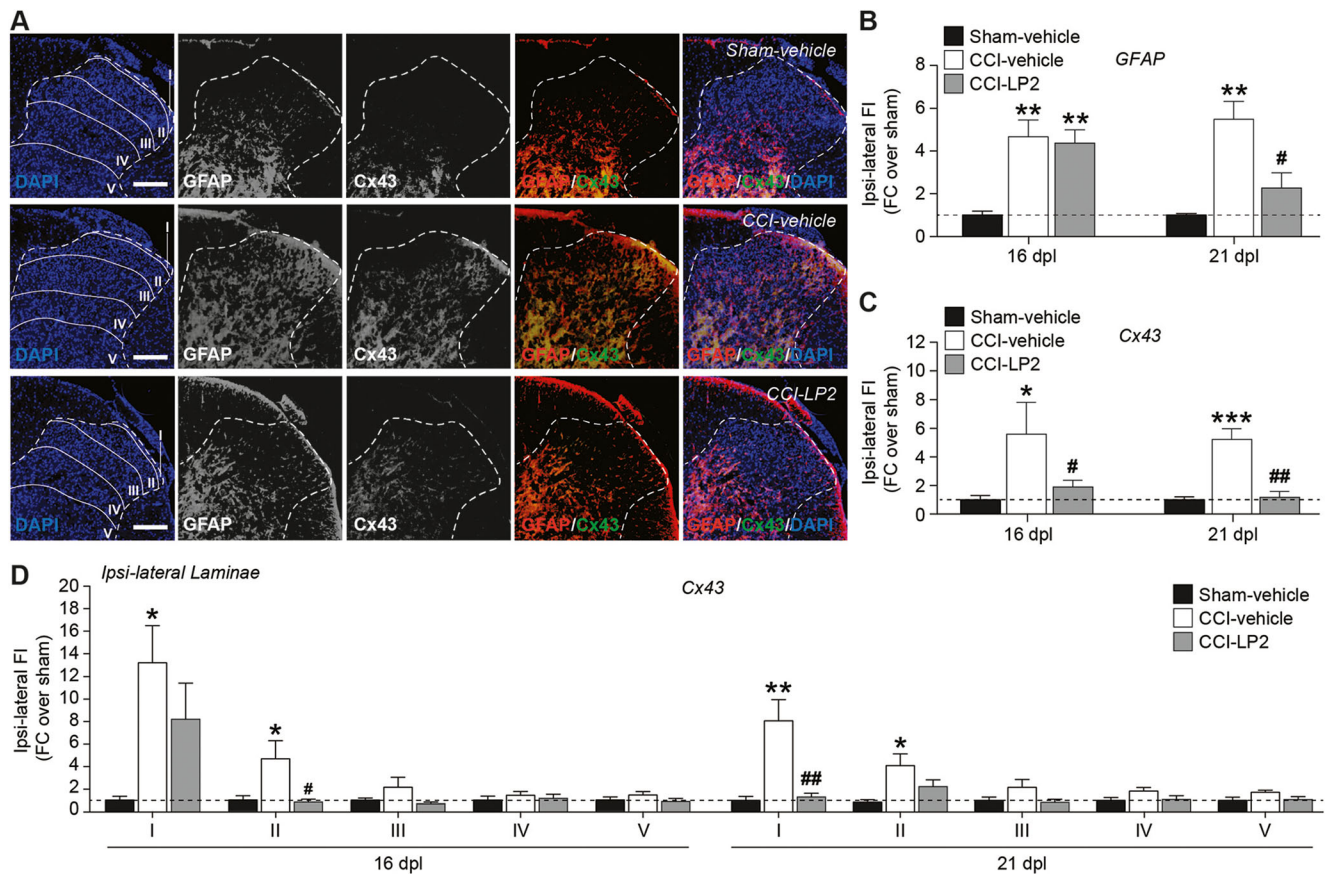
Fig. 4 MOR and DOR targeting with LP2 reduces GFAP and Cx43 levels in ipsi-lateral dorsal horns of CCI rats. **A** Representative images of ipsi-lateral dorsal horns of sham-vehicle, CCI-vehicle, and CCI-LP2 treated rats expressing Cx43 and GFAP at 21 dpl. Scale bars = 100 μm. **B**, **C** Quantification of GFAP (**B**) and Cx43 (**C**) fluorescence intensity in ipsi-lateral dorsal horns of sham-vehicle, CCI-vehicle, and CCI-LP2-treated rats. Data are shown as mean FC over sham-vehicle ± SEM of $n = 4$ rats per group. **D** Quantification of Cx43 fluorescence intensity in ipsi-lateral *laminae* I–V of dorsal horns of sham-vehicle, CCI-vehicle, and CCI-LP2-treated rats. Data are shown as mean FC over sham-vehicle ± SEM of $n = 4$ rats per group. Dpl, days post-ligatures; FI, fluorescence intensity; FC, fold change. *p value < 0.05, **p value < 0.01, and ***p value < 0.001 vs. sham-vehicle. #p value < 0.05 and ##p value < 0.01 vs. CCI-vehicle

0.7580 CCI-LP2 vs. sham-vehicle) and was significantly reduced at 21 dpl (0.8 ± 0.2 CCI-LP2 vs. 2.2 ± 0.4 CCI-vehicle, FC over sham-vehicle, $F_{treatment}(2, 6) = 9.465$; Fig. 5I).

These data confirm a significant and long-lasting modulation of astrogliosis mediated by the MOR/DOR ligand LP2, which was able to reduce astrogliosis at 21 dpl by reducing the reactive activation of Cx43 in dorsal horn *laminae* of the spinal cord from chronic neuropathic rats.

LP2 Reduces Cleaved Caspase 3-Positive Neurons in Ipsi-Lateral Dorsal Horn of CCI Rats

To confirm the neuroprotective effects of LP2 treatment during CCI-induced neuropathy, we assessed the Cl Casp3 signaling in the spinal cord dorsal horn. The total number of Cl Casp3-positive cells was reduced in ipsi-lateral dorsal horn at 16 dpl ($2.8 \pm 0.5\%$ CCI-LP2 vs. $6.0 \pm 0.4\%$ CCI-vehicle, $F_{treatment}(2, 6) = 29.23$) and at 21 dpl ($4.0 \pm 1.1\%$ CCI-LP2 vs. $8.6 \pm 0.9\%$ CCI-vehicle, $F_{treatment}(2, 6) = 16.36$; Fig. 6A–C). Quantification of the total number of Cl Casp3 and NeuN

double-positive cells confirmed that LP2 was able to reduce the percentage of neuronal pro-apoptotic cells at 16 dpl ($2.3 \pm 0.2\%$ CCI-LP2 vs. $3.5 \pm 0.1\%$ CCI-vehicle, $F_{treatment}(2, 6) = 86.75$) and 21 dpl ($2.0 \pm 0.4\%$ CCI-LP2 vs. $4.0 \pm 0.5\%$ CCI-vehicle, $F_{treatment}(2, 6) = 13.22$; Fig. 6D–F).

No significant differences were found in the contra-lateral cleaved caspase 3-positive cells and Cl Casp3 and NeuN double-positive cells at both 16 and 21 dpl (Fig. S5).

Discussion

Chronic neuropathic pain represents an unsolved challenge that needs new pharmacological approaches to overcome the limitations of currently available analgesics [18]. Classic MOR agonists have raised issue related to both limited analgesic effects and to paradoxical hyperalgesia and hostile cellular responses [34]. Beneficial and unwanted effects of MOR agonists are not limited to neurons and extend to glial cells [35]. Indeed, repeated morphine administrations lead to glial
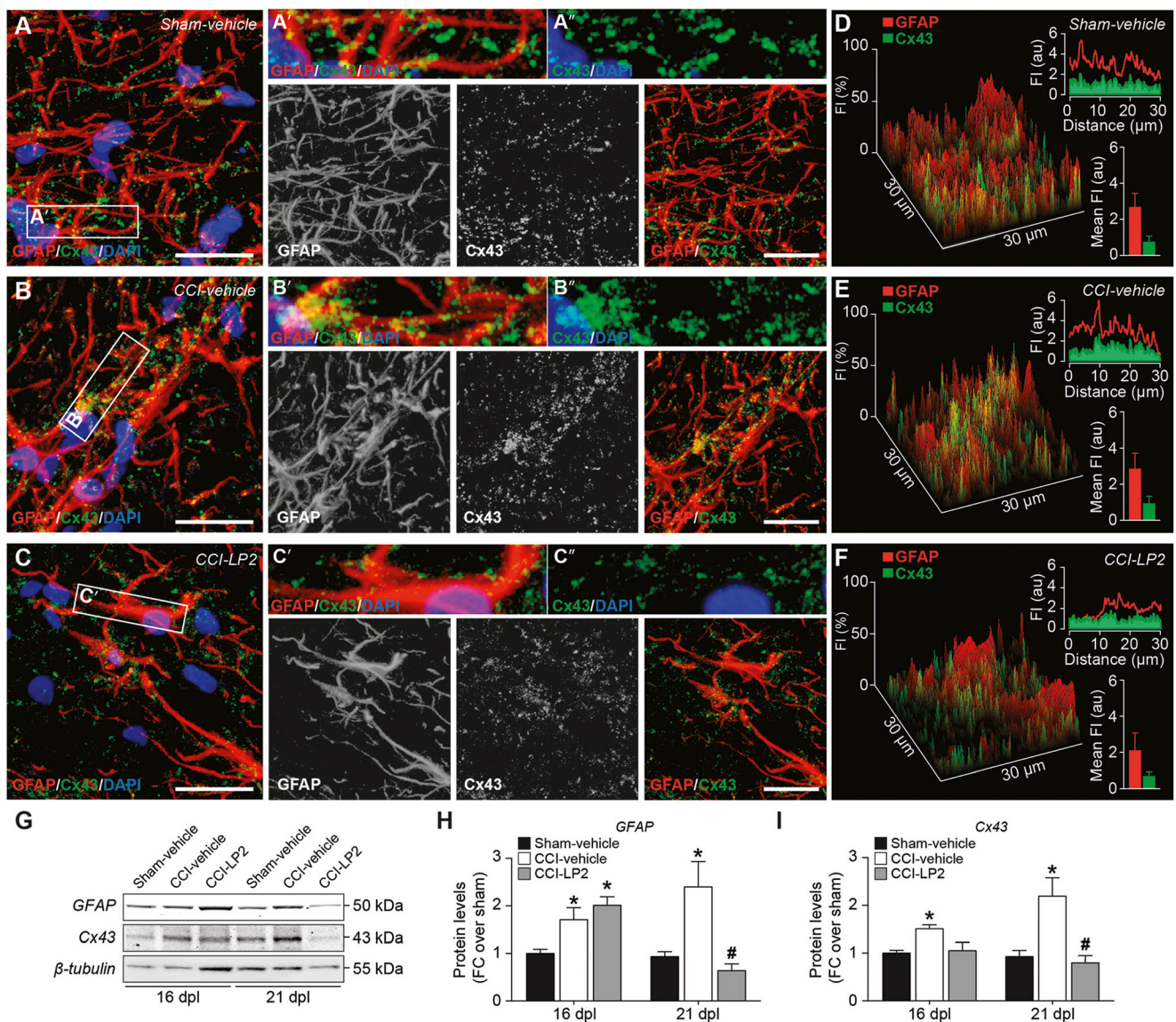
Fig. 5 LP2 reduces astrocytic Cx43 in ipsi-lateral dorsal horns of CCI rats. **A–C** Confocal microscopy images of GFAP-positive astrocytes in ipsi-lateral dorsal horns of sham-vehicle (**A**), CCI-vehicle (**B**), and CCI-LP2 (**C**) rats expressing Cx43 at 21 dpl. Panels **A′–A″**, **B′–B″**, and **C′–C″** show GFAP and Cx43 localization. Scale bars = 10 μm. **D–F** Surface plot and fluorescence intensity profile of confocal images in **A–C**. **G–I** Representative blots (**G**) and quantification of GFAP (**H**) and Cx43 (**I**) levels in the lumbar region of the spinal cords of sham-vehicle, CCI-vehicle, and CCI-LP2-treated rats at 16 and 21 dpl. Data are shown as mean FC over sham-vehicle ± SEM of $n = 3$ rats per group. FI, fluorescence intensity; au, arbitrary unit; dpl, days post-ligatures; FC, fold change. *p value < 0.05 vs. sham-vehicle and #p value < 0.05 vs. CCI-vehicle

cell activation and increase release of pro-inflammatory cytokines/chemokines, resulting in nociceptive transmission enhancement [36]. On the contrary, a number of evidences reported ameliorating effects mediated by DOR agonists in experimental neuropathies [20, 37, 38]. As such, DORs have been proposed as new targets in chronic pain and may exert a fundamental role in the chronicization processes. Moreover, DOR knockout mice show strengthened sensitization and intense increase of typical neurological features of neuropathic pain as compared to wild type, so that it is worth a careful analysis of the mechanisms underlying DOR activation [39,

40]. Interestingly, MOR and DOR co-localized in pain inhibitory pathways [41] and the existence of functional and physical cross-interactions between MOR and DOR have been established [42]. Nociceptive stimuli induce the slow, but persistent, DOR trafficking from the intracellular compartment, where normally stored, to the plasma membrane, which could increase receptor activation and promote MOR/DOR heterodimer formation [43, 44]. A number of evidences suggest that MOR activity could be modulated by DOR ligands increasing anti-nociceptive responses to MOR agonists or MOR signaling activation [45].
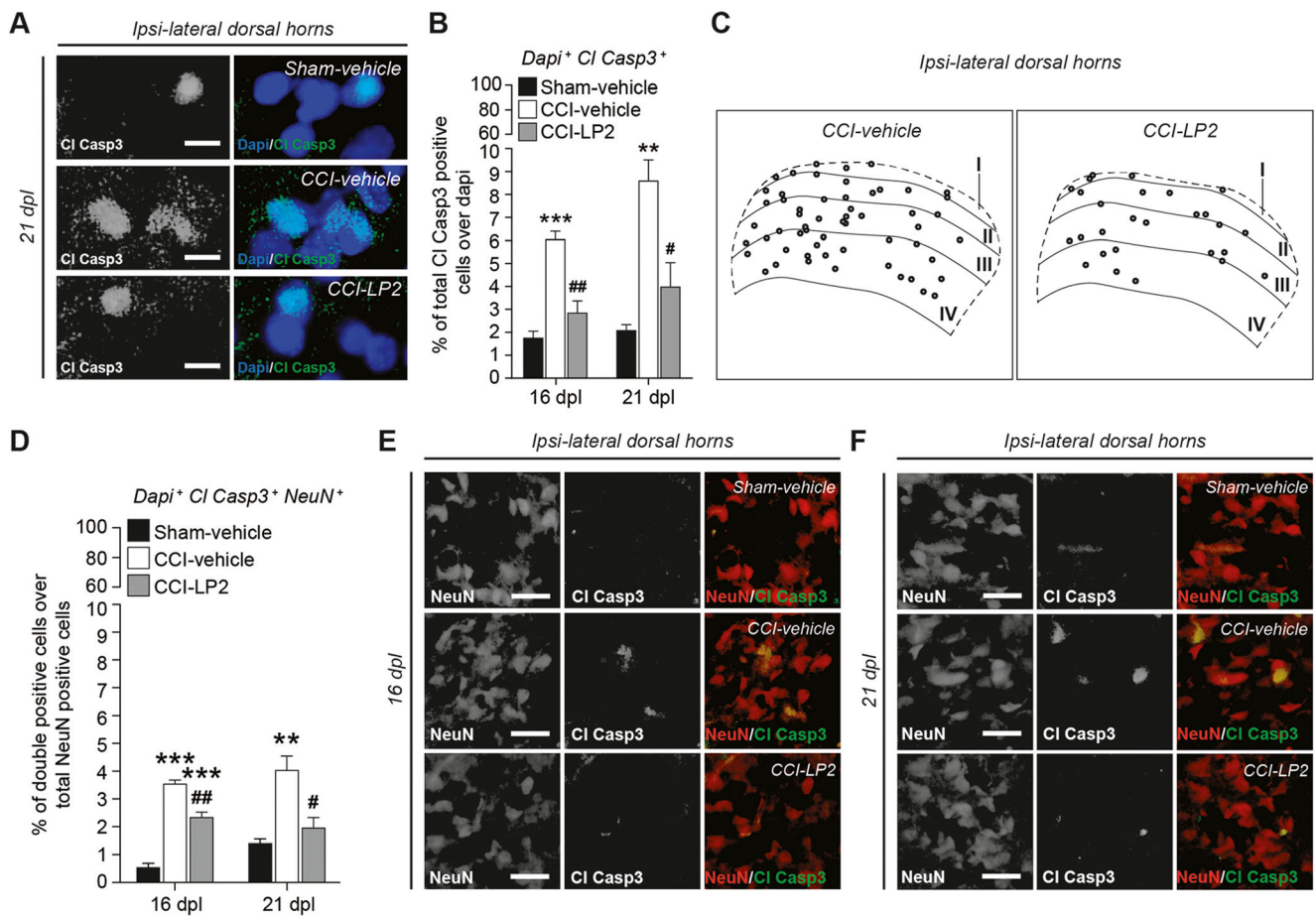
Fig. 6 LP2 reduces cleaved caspase 3-positive neurons in ipsi-lateral dorsal horns of CCI rats. **A**, **B** Representative images of Cl Casp3 immunofluorescence analysis at 21 dpl (**A**) and quantification (**B**) of Cl Casp3 and DAPI double cells over DAPI in ipsi-lateral dorsal horns of sham-vehicle, CCI-vehicle, and CCI-LP2-treated rats at 16 and 21 dpl. Data are shown as mean percentage ± SEM of $n = 3$ rats per group. Scale bars = 5 μm. **C** Reconstruction of the apoptotic profiles in the ipsi-lateral dorsal horn of CCI-vehicle versus CCI-LP2. Each dot represents a single Cl Casp3-positive DAPI-positive cell. **D–F** Quantification of the percentage of Cl Casp3- and NeuN double-positive cells (**D**) and representative images of Cl Casp3 and NeuN immunofluorescence analysis of ipsi-lateral dorsal horns at 16 dpl (**E**) and 21 dpl (**F**) of sham-vehicle, CCI-vehicle, and CCI-LP2 rats. Data are shown as mean ± SEM of $n = 3$ rats per group. Scale bars = 10 μm. Dpl, days post-ligatures; Cl Casp3, cleaved caspase 3. **p value < 0.01 and ***p value < 0.001 vs. sham-vehicle and #p value < 0.05 and ##p value < 0.01 vs. CCI-vehicle

Our study examined the molecular mechanisms underlying CCI-induced neuropathy and the effects of LP2 MOR/DOR targeting in neuroglia interactions as well as behavioral beneficial effects of this approach for the treatment of neuropathic pain. We showed that the repeated administration of the MOR/DOR ligand significantly inhibited the development of mechanical allodynia in neuropathic rats, increasing the withdrawal threshold as compared to CCI-vehicle rats up to 21 dpl. LP2 behavioral effects well related to its capability to simultaneously target and activate MOR and DOR. Bivalent ligands, containing the MOR agonist fentanyl and the DOR agonist enkephalin-like peptides, were developed as promising analgesics for treatment of neuropathic pain with an improved tolerability profile [46]. These effects relate with previous published evidences where mitragynine derivative MGM-16, possessing a MOR/DOR agonist profile, showed dose-dependent anti-allodynic effects in sciatic nerve-ligated

rats [47]. LP2 anti-allodynic effects in the CCI model of neuropathic pain could be also due to its prominent DOR component, whose role in neuropathy amelioration, through a reduced expression of pro-inflammatory cytokine TNF-α, has been previously demonstrated [37].

Several groups have showed that in the dorsal horns of neuropathic rats, a sustained pro-apoptotic signaling coexists with ROS and an increased glial-derived pro-inflammatory cytokine production [48–50]. Pro-inflammatory cytokines, resulting from direct insults to the nervous system, induce gap junctions and hemichannel activation, which has been proposed to be involved in neuroglia interactions [51–56]. Here, we found a significant increase of the proportion of pro-apoptotic spinal neurons in the ipsi-lateral dorsal horns of CCI rats, paired with reactive astrogliosis and robust Cx43 increase. By examining astrocyte response, a significant proportion of reactive astrocytes were found in *laminae* I and

II of CCI rats, where neurons expressing MORs and DORs mostly localize [41].

During the time course of neuropathic pain, both GFAP and Cx43 levels were increased from the early phases of chronic pain, suggesting that astroglial communication mediated by Cx43 plays a key role in promoting pain chronicization during neuropathies. These results were in line with several data showing Cx43 implication in secondary damages and inflammatory response during degenerative conditions including chronic neuropathic pain [9, 57, 58]. As such, Cx43 reveals the astroglial intensified communication as a consequence and/or as a primary warning of suffering conditions. In our setting, the multitarget opioid ligand LP2 reverted Cx43 levels earlier than GFAP astrogliosis, which is still ongoing after 5 days of treatment and significantly reduced only at 21 dpl. Thus, LP2-mediated Cx43 reduction seems to affect reactive astrogliosis upon neuropathies. Vice versa, evidences from literature report that chronic morphine treatment up-regulates the astrocytic spinal Cx43 expression responsible of the anti-nociceptive tolerance development in rats by activating N-methyl-D-aspartate (NMDA) receptors and inhibiting GLT-1 expression [59]. These results emphasize the LP2 effect on Cx43 that could be related to its peculiar opioid profile and are in accordance with the DOR contribution to infarct size limitation through the suppression of gap junction permeability by PKC-mediated Cx43 modulation [60]. Moreover, an increased expression of GFAP in the ventral tegmental area following prolonged systemic administration of morphine has been also demonstrated [36]. Taken together, these evidences suggest that multitarget MOR/DOR ligands, such as LP2, positively modulate MOR activity throughout G protein-mediated DOR activation [61].

The complex cause-effect relation including Cx43-mediated spread suffering and astrogliosis was also confirmed by our in vitro results. We found that LP2 exerts neuroprotective effects on over-stimulated DRG-derived neurons, which in turn were able to drive astrocyte responses. Spinal cord-derived astrocytes, exposed to conditioned media from picrotoxin-stimulated DRG-derived neurons, showed increased levels of Cx43 and reactive astrogliosis induced by astroglial modulating factors delivered by suffering neurons in the extracellular milieu. Despite a Cx43 reduction, no significant modifications of astrogliosis were observed upon MOR/DOR targeting on neuronal cultures. However, at mRNA level, we were able to detect a significant reduction of *Gfap* and a robust reduction of *Gja1* encoding for Cx43. This discrepancy in *Gfap* mRNA levels versus protein levels, not observed for *Gja1* mRNA encoding for Cx43, may also partially due to the relatively high protein turnover (i.e., few hours half-life) of connexins [53, 62], which allow cells to rapidly modulate Cxs protein levels. Astroglial cells were also actively expressing solute carrier family 1 member 2 and 3 (*slc1a2* and *slc1a3*) encoding for a high affinity glutamate transporter in both cultures exposed to the conditioned media from picrotoxin-stimulated and picrotoxin-stimulated LP2-treated neurons. Of note, slc1a2 is the principal glutamate transporter involved in synaptic glutamate clearance, playing crucial role in the glutamate uptake preventing excitotoxic neuronal damage [63, 64]. This indicates that over-stimulated neurons release soluble factors that induced reactive astrogliosis and that these factors are not present or at least reduced upon LP2 treatment, which exerts significant neuroprotective effects on neuronal cultures and consequential reduction of secondary damages on astrocytes. Taken together, these evidences confirm an effective repurposing of astrocytic phenotype upon LP2 treatment on neurons, indicating that MOR/DOR simultaneous targeting is not only neuroprotective for the target cell populations but reduced secondary damages on glial cells. Neuroglia axis is indeed influenced by modulators that may be different from neurotransmitters per se, establishing adaptation phenomena via soluble factors, extracellular vesicles and microRNAs [65–68]. Further studies are needed to characterize the magnitude of Cx43-inhibitory effect in neuropathic pain and the potential involvement of other molecular players that may interact in this axis.

In conclusion, here we showed that simultaneous MOR/DOR targeting leads to both analgesic and neuroprotective effects in a rodent model of neuropathic pain and that Cx43 plays a role in mediating reduction of reactive astrogliosis upon neuronal suffering. The effects relate to a reduction of neurological deficits upon peripheral injury and imply reduced reactive astrogliosis, anticipated by reduction of Cx43 levels from the early stages of the chronicization processes. These findings are paving the way for the development of new analgesic compounds with MOR/DOR profile as a new pharmacological strategy for the treatment of neuropathies and to prevent central sensitization.

Author Contributions NV, LP, RG, RP, CP: conceptualization; NV, LP, FMS, SC, FC, DT, RA, CP: investigation; NV, LP, SC, RT, FC, DT, RA, RG, RP, CP: formal analysis; NV, DT, RG, RP, CP: data curation; NV: wrote the manuscript—original editing; NV, RT, RG, RP, CP: reviewed and edited the manuscript. All authors read and approved the final manuscript.

Compliance with Ethical Standards

Conflict of Interest The authors declare no competing financial interests.

References

1. Campbell JN, Meyer RA (2006) Mechanisms of neuropathic pain. Neuron 52(1):77–92. https://doi.org/10.1016/j.neuron.2006.09.021

2. Nickel FT, Seifert F, Lanz S, Maihofner C (2012) Mechanisms of neuropathic pain. Eur Neuropsychopharmacol 22(2):81–91. https://doi.org/10.1016/j.euroneuro.2011.05.005

3. Latremoliere A, Woolf CJ (2009) Central sensitization: a generator of pain hypersensitivity by central neural plasticity. J Pain 10(9):895–926. https://doi.org/10.1016/j.jpain.2009.06.012

4. Gao YJ, Ji RR (2010) Targeting astrocyte signaling for chronic pain. Neurotherapeutics 7(4):482–493. https://doi.org/10.1016/j.nurt.2010.05.016

5. Tsuda M, Inoue K, Salter MW (2005) Neuropathic pain and spinal microglia: a big problem from molecules in 'small' glia. Trends Neurosci 28(2):101–107. https://doi.org/10.1016/j.tins.2004.12.002

6. Chen G, Park CK, Xie RG, Berta T, Nedergaard M, Ji RR (2014) Connexin-43 induces chemokine release from spinal cord astrocytes to maintain late-phase neuropathic pain in mice. Brain 137:2193–2209. https://doi.org/10.1093/brain/awu140

7. Chiang CY, Sessle BJ, Dostrovsky JO (2012) Role of astrocytes in pain. Neurochem Res 37(11):2419–2431. https://doi.org/10.1007/s11064-012-0801-6

8. Nagy JI, Dudek FE, Rash JE (2004) Update on connexins and gap junctions in neurons and glia in the mammalian nervous system. Brain Res Rev 47(1–3):191–215. https://doi.org/10.1016/j.brainresrev.2004.05.005

9. Bennett MV, Garre JM, Orellana JA, Bukauskas FF, Nedergaard M, Saez JC (2012) Connexin and pannexin hemichannels in inflammatory responses of glia and neurons. Brain Res 1487:3–15. https://doi.org/10.1016/j.brainres.2012.08.042

10. Retamal MA, Froger N, Palacios-Prado N, Ezan P, Saez PJ, Saez JC, Giaume C (2007) Cx43 hemichannels and gap junction channels in astrocytes are regulated oppositely by proinflammatory cytokines released from activated microglia. J Neurosci 27(50):13781–13792. https://doi.org/10.1523/Jneurosci.2042-07.2007

11. Orellana JA, Hernandez DE, Ezan P, Velarde V, Bennett MVL, Giaume C, Saez JC (2010) Hypoxia in high glucose followed by reoxygenation in normal glucose reduces the viability of cortical astrocytes through increased permeability of connexin 43 hemichannels. Glia 58(3):329–343. https://doi.org/10.1002/glia.20926

12. Vicario N, Calabrese G, Zappala A, Parenti C, Forte S, Graziano ACE, Vanella L, Pellitteri R et al (2017) Inhibition of Cx43 mediates protective effects on hypoxic/reoxygenated human neuroblastoma cells. J Cell Mol Med 21(10):2563–2572. https://doi.org/10.1111/jcmm.13177

13. Theriault E, Frankenstein UN, Hertzberg EL, Nagy JI (1997) Connexin43 and astrocytic gap junctions in the rat spinal cord after acute compression injury. J Comp Neurol 382(2):199–214

14. Cronin M, Anderson PN, Cook JE, Green CR, Becker DL (2008) Blocking connexin43 expression reduces inflammation and improves functional recovery after spinal cord injury. Mol Cell Neurosci 39(2):152–160. https://doi.org/10.1016/j.mcn.2008.06.005

15. Orellana JA, Saez PJ, Shoji KF, Schalper KA, Palacios-Prado N, Velarde V, Giaume C, Bennett MVL et al (2009) Modulation of brain hemichannels and gap junction channels by pro-inflammatory agents and their possible role in neurodegeneration. Antioxid Redox Sign 11(2):369–399. https://doi.org/10.1089/ars.2008.2130

16. Evans CJ, Keith DE, Morrison H, Magendzo K, Edwards RH (1992) Cloning of a delta opioid receptor by functional expression. Science 258(5090):1952–1955. https://doi.org/10.1126/science.1335167

17. Chen Y, Mestek A, Liu J, Yu L (1993) Molecular-cloning of a rat kappa-opioid receptor reveals sequence similarities to the mu-opioid and delta-opioid receptors. Biochemical J 295:625–628. https://doi.org/10.1042/bj2950625

18. Pasternak GW, Pan YX (2013) Mu opioids and their receptors: evolution of a concept. Pharmacol Rev 65(4):1257–1317. https://doi.org/10.1124/pr.112.007138

19. Chou R, Turner JA, Devine EB, Hansen RN, Sullivan SD, Blazina I, Dana T, Bougatsos C et al (2015) The effectiveness and risks of long-term opioid therapy for chronic pain: a systematic review for a National Institutes of Health Pathways to Prevention Workshop. Ann Intern Med 162(4):276–27+. https://doi.org/10.7326/M14-2559

20. Mika J, Przewlocki R, Przewlocka B (2001) The role of delta-opioid receptor subtypes in neuropathic pain. Eur J Pharmacol 415(1):31–37. https://doi.org/10.1016/S0014-2999(01)00814-7

21. Dietis N, Guerrini R, Calo G, Salvadori S, Rowbotham DJ, Lambert DG (2009) Simultaneous targeting of multiple opioid receptors: a strategy to improve side-effect profile. Brit J Anaesth 103(1):38–49. https://doi.org/10.1093/bja/aep129

22. Balboni G, Salvadori S, Trapella C, Knapp BI, Bidlack JM, Lazarus LH, Peng XM, Neumeyer JL (2010) Evolution of the bifunctional lead mu agonist/delta antagonist containing the 2',6'-dimethyl-L-tyrosine-1,2,3,4-tetrahydroisoquinoline-3-carboxylic acid (Dmt-Tic) opioid pharmacophore. ACS Chem Neurosci 1(2):155–164. https://doi.org/10.1021/cn900025j

23. Lowery JJ, Raymond TJ, Giuvelis D, Bidlack JM, Polt R, Bilsky EJ (2011) In vivo characterization of MMP-2200, a mixed delta/mu opioid agonist, in mice. J Pharmacol Exp Ther 336(3):767–778. https://doi.org/10.1124/jpet.110.172866

24. George SR, Fan T, Xie ZD, Tse R, Tam V, Varghese G, O'Dowd BF (2000) Oligomerization of mu- and delta-opioid receptors—generation of novel functional properties. J Biol Chem 275(34):26128–26135. https://doi.org/10.1074/jbc.M000345200

25. Pasquinucci L, Turnaturi R, Prezzavento O, Arena E, Arico G, Georgoussi Z, Parenti R, Cantarella G et al (2017) Development of novel LP1-based analogues with enhanced delta opioid receptor profile. Bioorgan Med Chem 25(17):4745–4752. https://doi.org/10.1016/j.bmc.2017.07.021

26. Pasquinucci L, Turnaturi R, Montenegro L, Caraci F, Chiechio S, Parenti C (2019) Simultaneous targeting of MOR/DOR: a useful strategy for inflammatory pain modulation. Eur J Pharmacol 847:97–102. https://doi.org/10.1016/j.ejphar.2019.01.031

27. Pasquinucci L, Turnaturi R, Calò G, Pappalardo F, Ferrari F, Russo G, Arena E, Montenegro L, Chiechio S, Prezzavento O, Parenti C (2019) (2S)-N-2-methoxy-2-phenylethyl-6,7-benzomorphan compound (2S-LP2): Discovery of a biased mu/delta opioid receptor agonist. Eur J Med Chem. https://doi.org/10.1016/j.ejmech.2019.02.043

28. Bennett GJ, Xie YK (1988) A peripheral mononeuropathy in rat that produces disorders of pain sensation like those seen in man. Pain 33(1):87–107. https://doi.org/10.1016/0304-3959(88)90209-6

29. Parenti C, Turnaturi R, Arico G, Gramowski-Voss A, Schroeder OH, Marrazzo A, Prezzavento O, Ronsisvalle S et al (2013) The multitarget opioid ligand LP1's effects in persistent pain and in primary cell neuronal cultures. Neuropharmacology 71:70–82. https://doi.org/10.1016/j.neuropharm.2013.03.008

30. Parenti C, Marrazzo A, Arico G, Parenti R, Pasquinucci L, Ronsisvalle S, Ronsisvalle G, Scoto GM (2014) The antagonistic effect of the sigma 1 receptor ligand (+)-MR200 on persistent pain induced by inflammation. Inflamm Res 63(3):231–237. https://doi.org/10.1007/s00011-013-0692-2

31. Dixon WJ (1980) Efficient analysis of experimental observations. Annu Rev Pharmacol Toxicol 20:441–462. https://doi.org/10.1146/annurev.pa.20.040180.002301

32. Gumy LF, Bampton ETW, Tolkovsky AM (2008) Hyperglycaemia inhibits Schwann cell proliferation and migration and restricts regeneration of axons and Schwann cells from adult murine DRG. Mol Cell Neurosci 37(2):298–311. https://doi.org/10.1016/j.mcn.2007.10.004

33. Avola R, Condorelli DF, Turpeenoja L, Ingrao F, Reale S, Ragusa N, Stella AMG (1988) Effect of epidermal growth-factor on the labeling of the various rna species and of nuclear proteins in primary rat astroglial cell-cultures. Journal of Neuroscience Research 20(1):54–63. https://doi.org/10.1002/jnr.490200109

34. Brush DE (2012) Complications of long-term opioid therapy for management of chronic pain: the paradox of opioid-induced hyperalgesia. J Med Toxicol 8(4):387–392. https://doi.org/10.1007/s13181-012-0260-0

35. Beitner-Johnson D, Nestler EJ (1991) Morphine and cocaine exert common chronic actions on tyrosine hydroxylase in dopaminergic brain reward regions. J Neurochem 57(1):344–347

36. Goins EC, Bajic D (2018) Astrocytic hypertrophy in the rat ventral tegmental area following chronic morphine differs with age. J Neurol Neurorehabilit Res 3(1):14–21

37. Vicario N, Parenti R, Arico G, Turnaturi R, Scoto GM, Chiechio S, Parenti C (2016) Repeated activation of delta opioid receptors counteracts nerve injury-induced TNF-alpha up-regulation in the sciatic nerve of rats with neuropathic pain: a possible correlation with delta opioid receptors-mediated antiallodinic effect. Mol Pain 12: 174480691666794. https://doi.org/10.1177/1744806916667949

38. Pradhan AA, Befort K, Nozaki C, Gaveriaux-Ruff C, Kieffer BL (2011) The delta opioid receptor: an evolving target for the treatment of brain disorders. Trends Pharmacol Sci 32(10):581–590. https://doi.org/10.1016/j.tips.2011.06.008

39. Gaveriaux-Ruff C, Nozaki C, Nadal X, Hever XC, Weibel R, Matifas A, Reiss D, Filliol D et al (2011) Genetic ablation of delta opioid receptors in nociceptive sensory neurons increases chronic pain and abolishes opioid analgesia. Pain 152(6):1238–1248. https://doi.org/10.1016/j.pain.2010.12.031

40. Nadal X, Banos JE, Kieffer BL, Maldonado R (2006) Neuropathic pain is enhanced in delta-opioid receptor knockout mice. Eur J Neurosci 23(3):830–834. https://doi.org/10.1111/j.1460-9568.2006.04569.x

41. Wang D, Tawfik VL, Corder G, Low SA, Francois A, Basbaum AI, Scherrer G (2018) Functional divergence of delta and mu opioid receptor organization in CNS pain circuits. Neuron 98(1):90–108 e105. https://doi.org/10.1016/j.neuron.2018.03.002

42. Zhang X, Bao L, Li S (2015) Opioid receptor trafficking and interaction in nociceptors. Br J Pharmacol 172(2):364–374. https://doi.org/10.1111/bph.12653

43. Cahill CM, Holdridge SV, Morinville A (2007) Trafficking of delta-opioid receptors and other G-protein-coupled receptors: implications for pain and analgesia. Trends Pharmacol Sci 28(1):23–31. https://doi.org/10.1016/j.tips.2006.11.003

44. van Rijn RM, Whistler JL, Waldhoer M (2010) Opioid-receptor-heteromer-specific trafficking and pharmacology. Curr Opin Pharmacol 10(1):73–79. https://doi.org/10.1016/j.coph.2009.09.007

45. Levitt ES, Purington LC, Traynor JR (2011) Gi/o-coupled receptors compete for signaling to adenylyl cyclase in SH-SY5Y cells and reduce opioid-mediated cAMP overshoot. Mol Pharmacol 79(3):461–471. https://doi.org/10.1124/mol.110.064816

46. Podolsky AT, Sandweiss A, Hu J, Bilsky EJ, Cain JP, Kumirov VK, Lee YS, Hruby VJ et al (2013) Novel fentanyl-based dual mu/delta-opioid agonists for the treatment of acute and chronic pain. Life Sci 93(25–26):1010–1016. https://doi.org/10.1016/j.lfs.2013.09.016

47. Matsumoto K, Narita M, Muramatsu N, Nakayama T, Misawa K, Kitajima M, Tashima K, Devi LA et al (2014) Orally active opioid mu/delta dual agonist MGM-16, a derivative of the indole alkaloid mitragynine, exhibits potent antiallodynic effect on neuropathic pain in mice. J Pharmacol Exp Ther 348(3):383–392. https://doi.org/10.1124/jpet.113.208108

48. Raghavendra V, Rutkowski MD, DeLeo JA (2002) The role of spinal neuroimmune activation in morphine tolerance/hyperalgesia in neuropathic and sham-operated rats. J Neurosci 22(22):9980–9989

49. Watkins LR, Hutchinson MR, Johnston IN, Maier SF (2005) Glia: novel counter-regulators of opioid analgesia. Trends Neurosci 28(12):661–669. https://doi.org/10.1016/j.tins.2005.10.001

50. Gong N, Li XY, Xiao Q, Wang YX (2014) Identification of a novel spinal dorsal horn astroglial D-amino acid oxidase-hydrogen peroxide pathway involved in morphine antinociceptive tolerance. Anesthesiology 120(4):962–975. https://doi.org/10.1097/ALN.0b013e3182a66d2a

51. Froger N, Orellana JA, Calvo CF, Amigou E, Kozoriz MG, Naus CC, Saez JC, Giaume C (2010) Inhibition of cytokine-induced connexin43 hemichannel activity in astrocytes is neuroprotective. Mol Cell Neurosci 45(1):37–46. https://doi.org/10.1016/j.mcn.2010.05.007

52. Jeon YH, Youn DH (2015) Spinal gap junction channels in neuropathic pain. Korean J Pain 28(4):231–235. https://doi.org/10.3344/kjp.2015.28.4.231

53. Vicario N, Zappala A, Calabrese G, Gulino R, Parenti C, Gulisano M, Parenti R (2017) Connexins in the central nervous system: physiological traits and neuroprotective targets. Front Physiol 8:1060. https://doi.org/10.3389/fphys.2017.01060

54. Zappala A, Parenti R, La Delia F, Cicirata V, Cicirata F (2010) Expression of connexin57 in mouse development and in harmaline-tremor model. Neuroscience 171(1):1–11. https://doi.org/10.1016/j.neuroscience.2010.09.010

55. Parenti R, Cicirata F, Zappala A, Catania A, La Delia F, Cicirata V, Tress O, Willecke K (2010) Dynamic expression of Cx47 in mouse brain development and in the cuprizone model of myelin plasticity. Glia 58(13):1594–1609. https://doi.org/10.1002/glia.21032

56. Cicirata F, Parenti R, Spinella F, Giglio S, Tuorto F, Zuffardi O, Gulisano M (2000) Genomic organization and chromosomal localization of the mouse Connexin36 (mCx36) gene. Gene 251(2):123–130

57. Chen M, Kress B, Han X, Moll K, Peng W, Ji RR, Nedergaard M (2013) Astrocytic Cx43 hemichannels and gap junctions play a crucial role in development of chronic neuropathic pain following spinal cord injury. Glia 61:S212–S212

58. Orellana JA, Stehberg J (2014) Hemichannels: new roles in astroglial function. Front Physiol 5:193. https://doi.org/10.3389/fphys.2014.00193

59. Shen N, Mo LQ, Hu F, Chen PX, Guo RX, Feng JQ (2014) A novel role of spinal astrocytic connexin 43: mediating morphine antinociceptive tolerance by activation of NMDA receptors and inhibition of glutamate transporter-1 in rats. Cns Neuroscience & Therapeutics 20(8):728–736. https://doi.org/10.1111/cns.12244

60. Miura T, Yano T, Naitoh K, Nishihara M, Miki T, Tanno M, Shimamoto K (2007) Delta-opioid receptor activation before ischemia reduces gap junction permeability in ischemic myocardium by PKC-epsilon-mediated phosphorylation of connexin 43. Am J Physiol Heart Circ Physiol 293(3):H1425–H1431. https://doi.org/10.1152/ajpheart.01115.2006

61. Gendron L, Mittal N, Beaudry H, Walwyn W (2015) Recent advances on the delta opioid receptor: from trafficking to function. Br J Pharmacol 172(2):403–419. https://doi.org/10.1111/bph.12706

62. Beardslee MA, Laing JG, Beyer EC, Saffitz JE (1998) Rapid turnover of connexin43 in the adult rat heart. Circ Res 83(6):629–635

63. Danbolt NC (2001) Glutamate uptake. Prog Neurobiol 65(1):1–105

64. Rothstein JD, Martin L, Levey AI, Dykes-Hoberg M, Jin L, Wu D, Nash N, Kuncl RW (1994) Localization of neuronal and glial glutamate transporters. Neuron 13(3):713–725

65. Zhuang ZY, Gerner P, Woolf CJ, Ji RR (2005) ERK is sequentially activated in neurons, microglia, and astrocytes by spinal nerve ligation and contributes to mechanical allodynia in this neuropathic pain model. Pain 114(1–2):149–159. https://doi.org/10.1016/j.pain.2004.12.022

66. Zhao P, Waxman SG, Hains BC (2007) Extracellular signal-regulated kinase-regulated microglia-neuron signaling by prostaglandin E2 contributes to pain after spinal cord injury. J Neurosci 27(9):2357–2368. https://doi.org/10.1523/JNEUROSCI.0138-07.2007

67. Manzhulo IV, Ogurtsova OS, Kipryushina YO, Latyshev NA, Kasyanov SP, Dyuizen IV, Tyrtyshnaia AA (2016) Neuron-astrocyte interactions in spinal cord dorsal horn in neuropathic pain development and docosahexaenoic acid therapy. J Neuroimmunol 298:90–97. https://doi.org/10.1016/j.jneuroim.2016.07.015

68. Simeoli R, Montague K, Jones HR, Castaldi L, Chambers D, Kelleher JH, Vacca V, Pitcher T et al (2017) Exosomal cargo including microRNA regulates sensory neuron to macrophage communication after nerve trauma. Nat Commun 8(1):1778. https://doi.org/10.1038/s41467-017-01841-5